Design of Experiment Analysis on Multiple PIM Sources in an RF Antenna System

Shengxuan Xia^{#1}, Yuchu He^{*2}, Haicheng Zhou^{*3}, Hanfeng Wang^{*4} and Chulsoon Hwang^{#5}

*EMC Laboratory, Missouri University of Science and Technology, Rolla, MO, USA

*Google LLC, Mountain View, CA, USA

**Isx7c3, **5hwange@mst.edu

Abstract— Passive intermodulation (PIM) has been identified as one of the common root causes for receiving sensitivity degradation (desense) on radio-frequency (RF) antennas working in frequency-division duplex mode. The component-level PIM characterization and simulation have been well-established over the years. However, the study has been using an ideal 50 Ω transmission line system while antenna modules are more complicated than a simple transmission line structure. Moreover, the metallic contacts can exist in multiple locations with different connection topologies in real applications. This paper provides a method to simulate the PIM performance caused by the metallic contacts in a practical environment. In addition, the design of experiment (DoE) analysis is conducted to understand the statistical relationship between the component nonlinearity and the total PIM levels. Prioritizing the critical contact locations design insights including what-if scenario studies are found with the DoE.

Keywords— Design of experiment, desense, radio frequency, antenna, passive intermodulation.

I. INTRODUCTION

With the increasing trend of compact designs and high-speed wireless communications on consumer electronic devices, radio-frequency (RF) interference has become a common engineering consideration [1]. The interfering spectrum, generated by the nearby integrated circuits (ICs) modules or channels, may contaminate the receiving band of an RF antenna and thus cause desense problems [2-5]. Those straightforward RF interference problems have been well studied over the years with clear modeling methods for noise source and coupling path [6,7]. However, passive intermodulation (PIM) has been identified as another mechanism for desense problems that have higher complexity [8]. In frequency-division duplex (FDD) mode operating wireless systems, PIM can cause spectrum leakage from the high-power transmitting (TX) signals to the receiving (RX) channels. Non-ideal metallic contacts are the potential PIM sources due to the existence of a thin oxide layer between the contact interfaces [9,10]. Researchers have spent significant efforts in PIM modeling of the standard RF accessories [11-14], but those components or devices do not have a direct relationship to consumer electronic products. As the involved metallic components in the electronic devices (such as springs, gaskets, and conductive foams/tapes) are not coaxial

structures, a special test fixture is needed to conduct the component-level PIM characterizations [15].

When it comes to the system-level PIM or desense estimation, there are two more challenging parts: 1) those components show significant variations in PIM performance because of multiple factors such as manufacturing tolerance [16], material defects [17], mechanical conditions [18], etc., and 2) multiple metallic contacts are involved in an RF antenna module. These two factors make the practical PIM analysis more challenging. However, this multiple-PIM-source scenario can be converted into a statistical problem with multiple continuous random variables (potential random level PIM sources) and one response (total PIM at the antenna port). Design of experiment (DoE) is suitable for conducting screening and analyzing the effects of multiple variables on the response [19]. Thus, with the appropriate nonlinear modeling method and DoE, the practical PIM study with multiple PIM sources can be readily conducted.

In this paper, the component-level nonlinearity modeling is introduced. Then, for the complete RF antenna module, an equivalent circuit model (with the potential PIM source's locations preserved) is extracted from a full-wave simulation. Plugging the nonlinear components into the circuit model the system-level PIM is estimated as running a circuit simulation. With DoE, statistical analysis is conducted. The criticalness of each PIM source is prioritized, which can serve as guidance for engineers to mitigate the PIM-caused desense problems.

II. EQUIVALENT CIRCUIT WITH MULTIPLE PIM SOURCES

As discussed, an RF antenna module can consist of multiple potential PIM sources. To comprehensively model the entire antenna module with both the electromagnetic (EM) characteristics and the nonlinearity, a full-wave simulation is required with some specific handlings (discussed in subsection B). A simplified polynomial expression of the I-V curve is used to represent the nonlinear property of each individual metallic contact component. The nonlinearity level can be tuned by adjusting the corresponding polynomial coefficients. Then those nonlinear components can be plugged into the full-wave simulated model for the system-level PIM study.

This work was supported in part by the National Science Foundation (NSF) under Grant IIP-1916535.

A. Component-level PIM Representation

For the nonlinearity representation of the metallic contacts, polynomial expansion of the I-V relationship is a straightforward and intrinsic method. The voltage expressed in terms of current is written as:

$$V_{\text{out}} = a_0 + a_1 I_{\text{in}} + a_2 I_{\text{in}}^2 + a_3 I_{\text{in}}^3 + \cdots$$
 (1)

As the interested nonlinearity in PIM only includes the sideband frequency components, all the even order coefficients in (1) can be omitted. Furthermore, most of the PIM related studies use two-tone injection (to mimic the TX signal) and use the 3rd order inter-modulated product (IM3) to serve as a figure-of-merit for nonlinearity level representation [15]. Thus, the polynomial expression can be further reduced as:

$$V_{\text{out}} = a_1 I_{\text{in}} + a_3 I_{\text{in}}^3 \tag{2}$$

When two-tone $(f_1, f_2, \text{ and } f_1 < f_2)$ mimics the TX, the equation is changed to:

$$I_{in}(t) = I_0 \cos 2\pi f_1 t + I_0 \cos 2\pi f_2 t \tag{3}$$

$$V_{\text{out}}(t) = a_1 I_0(\cos 2\pi f_1 t + \cos 2\pi f_2 t) + a_3 I_0^3(\cos^3 2\pi f_1 t + \cos^3 2\pi f_2 t + 3\cos^2 2\pi f_1 t \cdot \cos 2\pi f_2 t + 3\cos^2 2\pi f_1 t \cdot \cos 2\pi f_1 t),$$
(4)

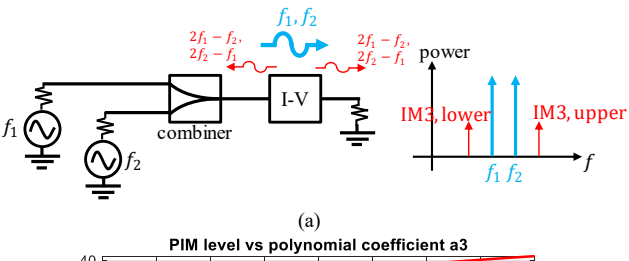
where I_0 is the current amplitude of each tone. As Fig. 1 (a) shows, the two equal-power sinusoidal waves are combined and injected into the nonlinear I-V, and the sideband is therefore generated. Thus, the IM3 product can be found as:

$$V_{\text{IM3, upper}}(t) = \frac{3}{4} a_3 I_0^3 \cos(2\pi (2f_2 - f_1)t), \tag{5}$$

and the lower side IM3 product $(2f_1 - f_2)$ is expressed similarly as (5). Given a constant amplitude of the input RF current, the nonlinearity created IM3 level is determined by the coefficient a_3 . In other words, a_3 can be a tunable variable to provide the I-V component with different levels of nonlinearity (demonstrated in Fig. 1 (b)). This nonlinear I-V method has been adopted as one of the effective ways to correlate with PIM performance experimentally [20]. It is worth to emphasize that this I-V representation in (3) assumes no reflection (or negligible) of the TX signal along the RF path. Fortunately, this is usually a reasonable assumption because the metallic contacts often have very small impedance.

B. Full-wave Extraction Workflow

In the RF antenna modules, however, the scenario with multiple PIM sources involved is more sophisticated. In Fig. 2 (a), for example, the antenna system consists of the antenna structure (embedded on the edge of the chassis frame) and the tuning circuits on flexible PCBs. Therefore, the RF current flow is more complicated than a transmission line system with a matched termination. Moreover, the metallic contact components are scattered at different locations and serve different purposes: in this example, the fork-shaped springs are for grounding purpose to connect the flexible PCB return planes with the metal chassis ground (Fig. 2 (b), shunt connections in the antenna circuit), while the pad-ring receptacles with screws



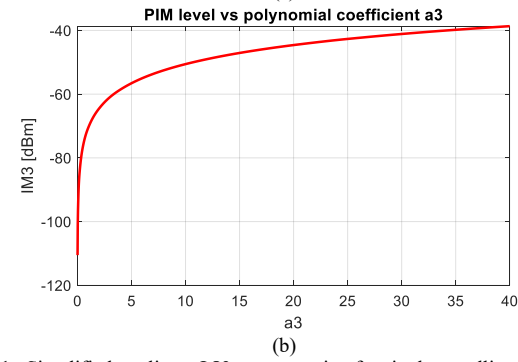


Fig. 1. Simplified nonlinear I-V representation for single metallic contact: (a) two-tone based method for quantification of nonlinearity; (b) IM3 vs 3rd order relymomial coefficient.

Chassis ground

Antenna feeding port

Potential PIM sources

RF antenna

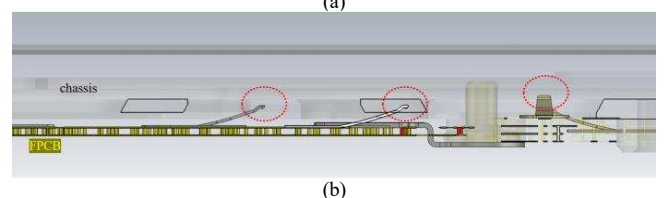


Fig. 2. Illustration of an RF antenna module with multiple potential PIM sources: (a) top view; (b) cutting plane cross-sectional view.

connect the antenna structure with the flexible PCBs (series connections).

A full-wave simulation is required to correctly represent the EM characteristics of the entire antenna system. This step is the most time-consuming part due to the high complexity [21], but only need to be done once. However, all the metallic contact locations should be preserved as lumped ports for the later insertions of nonlinear I-V blocks. The detailed handlings of the contacts are illustrated in Fig. 3. It is worth noting that although the port definitions have slight offset to the actual PIM source locations (e.g., only the tiny spring tip is the location of actual dominant PIM generation but the full-wave model cuts away a longer segment to insert the port), the metallic components are electrically small because their dimensions are within millimeter range. The eventual full-wave model of the entire antenna

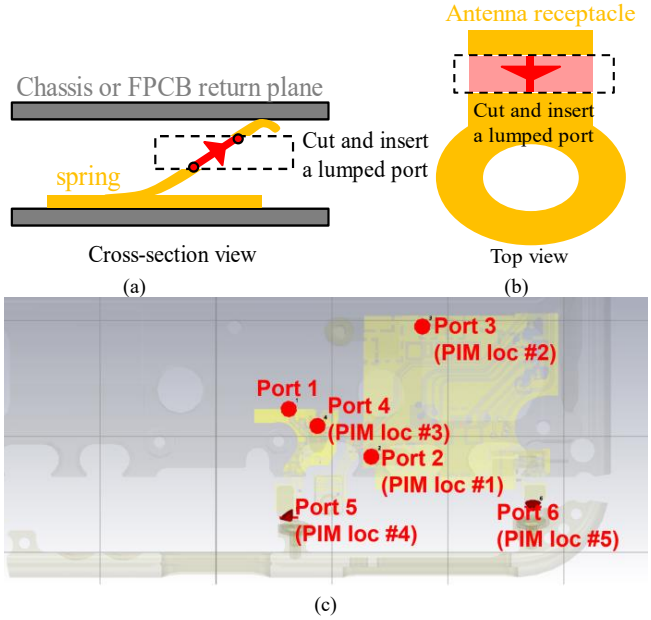


Fig. 3. Full-wave simulation model explanation: (a) handling of the spring contact locations; (b) handling of the pad-ring receptacles; (c) all the ports in the antenna module.

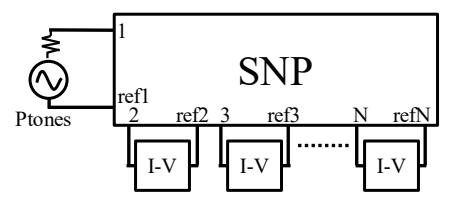


Fig. 4. Extracted equivalent circuit model for system-level PIM estimations.

system is shown in Fig. 3 (c), port 1 is the coaxial cable connection location to the antenna, and ports 2~6 are preserved for 5 potential PIM locations.

Because all the potential PIM source locations are defined as $50~\Omega$ ports, the simulation can generate multi-port S-parameters for post-processing. Except for the one port used for RF current injection, all the other ports can be plugged in with the nonlinear I-V block discussed in Section II. A (Fig. 4). With the equivalent circuit model extracted from a full-wave simulation, the system-level PIM estimation is as simple as running a circuit simulation (e.g., Harmonic Balance solver in ADS, or other equivalent tools) with any combinations of the nonlinear I-V blocks. The generated PIM power is observed at port 1. The extracted S-parameters can be re-used over and over to investigate different contact quality scenarios. This enables a faster simulator that can generate massive data for statistical analysis.

III. DOE ANALYSIS ON MULTIPLE TUNABLE PIM SOURCES

As discussed in Section II, each nonlinear component can be nonlinearity-tunable and be plugged into the equivalent circuit model for fast system-level PIM simulation. Therefore, the multiple PIM analysis can be considered as a scenario with multiple input variables and one output response. Statistical methods such as DoE can be utilized as a tool for this study.

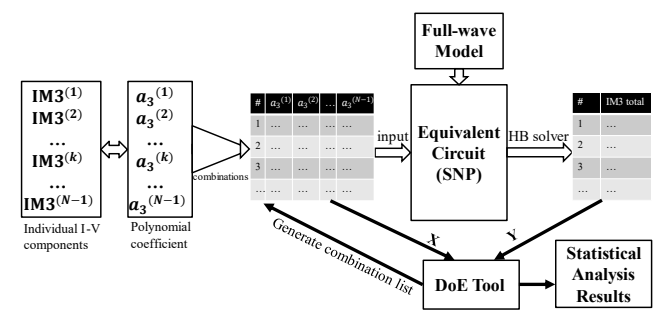


Fig. 5. Statistical data generation workflow.

A. Statistical Data Generation Process

Once the most time-consuming full-wave simulation is finished, the extracted S-parameters allow fast circuit simulations to generate massive amounts of data for the statistical study. As shown in Fig. 5, the 3rd order polynomial coefficients of the individual potential PIM sources can function as random variables to represent different PIM levels of each contact (discussed in Section II. A), then the DoE tool (for example, DoE function embedded in ADS, or more sophisticated tools like JMP) can provide a list of variable combinations for the simulator to run all those given cases (can be understood as a batch simulation). After obtaining the responses for all the cases, a full list with both inputs and output can be put back into the DoE tool for statistical result analysis.

There are five PIM sources of interest (Fig. 3) in this antenna module example. All the coefficients of a_1 were set to be fixed value of 0.2 (for demonstration purposes, so any small number indicating a lower than 1 Ω resistance should be reasonable). The range of the coefficients a_3 of all the PIM components range from 0.1 to 40 (same as in Fig. 1 (b)). The total generated PIM power of the entire antenna module can be found easily for every combination of the coefficients.

B. DoE Analysis of the Statistical Results

With all the random combinations of the coefficients and the corresponding responses obtained, statistical analysis can be conducted. Firstly, the Pareto results can be generated to prioritize the importance of the factors. As shown in Fig. 6, PIM locations #3 and #4 are the most dominant contributors while the other PIM sources have a much weaker impact on the total PIM.

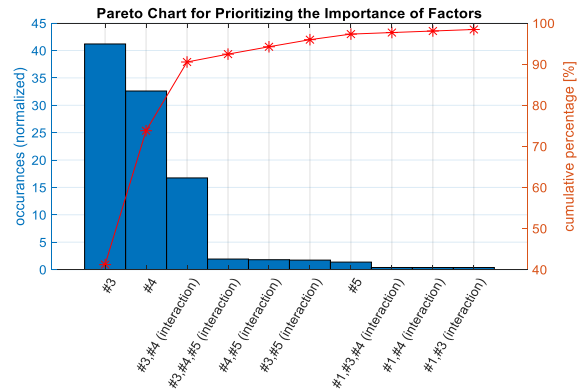
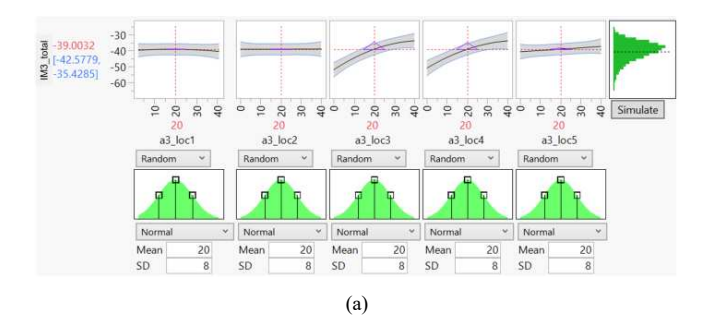
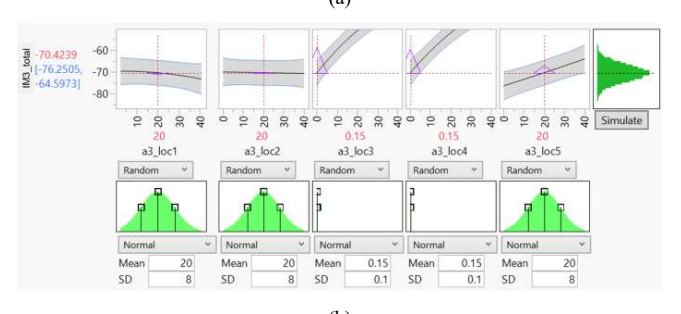


Fig. 6. Pareto chart result of multiple PIM source locations.





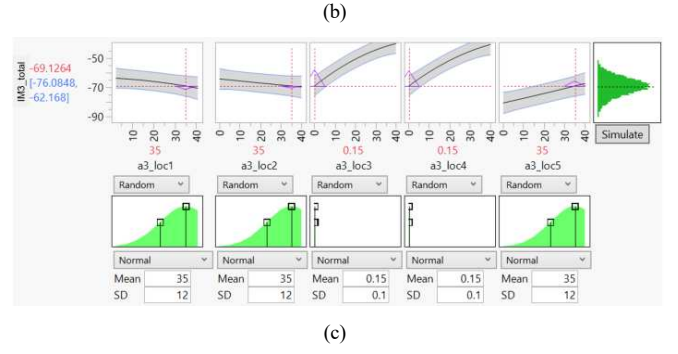


Fig. 7. DoE analysis results under different configurations: (a) original case, all PIM sources are poor; (b) only the two critical sources are mitigated; (c) the two critical sources mitigated, while all the others are intentionally worse.

Furthermore, the DoE tool has the capabilities for the distribution analysis and what-if scenario predictions. For example, in Fig. 7 (a), the original case, all the cursors were placed at the middle values. If the random variables are specified with certain distributions (for demonstration purpose only here, use Gaussian distributions, but can be other random distributions), the distribution of the output PIM result can be found. If the two dominant PIM sources are mitigated (a_3 values at location #3 and #4 are reduced), the mean value and the distribution of the output IM3 are changed accordingly, shown in Fig. 7 (b). The mean value out IM3 is changed from -39 dBm to -70.4 dBm (31.4 dB reduction), and under this configuration, the PIM location #5 shows higher sensitivity than the other two PIM sources #1 and #2, but still negligible comparing to the two dominant sources (which is consistent with the results in Fig. 6). Moreover, if the two dominant PIM sources are mitigated while all the other PIM sources are intentionally created to be poor contacts (in other words, even higher PIM), the output IM3 result almost remains the same (less than 1.4 dB difference), as shown in Fig. 7 (c).

From those DoE analysis results, in this multiple PIM antenna system, effective and significant desense mitigation can

be achieved by only solving for the critical PIM sources, even if the other PIM locations have poor contact qualities. What-if scenarios can be quickly determined by adjusting the variables. The yield can also be determined with the distribution results (e.g., in Fig. 7 (b), with 84% confidence that the IM3 is below -64.6 dBm level).

C. Discussions

This workflow is purely simulation based because it is practically difficult to preserve the ports in measurements. So, this is more suitable in a pre-design stage for quick desense criticalness evaluations. Significant efforts and costs can be reduced by only focusing on the critical contact locations (such as gold-plating treatment only at specific locations).

In the entire workflow, however, some aspects require attention:

- The random variable sampling: the individual IM3 level vs a_3 shows a nonlinear relationship, so a non-uniform sampling in a_3 is preferred.
- Distributions: in this study, for demonstration purposes, we simply assumed the Gaussian distributions with certain mean and standard deviation values. To better mimic the real situation, the actual distributions may be found experimentally with the component-level characterization setup [22] under various contact forces.
- Limitation: this method only applies to discrete PIM sources. The port definitions make sense only when the metallic contacts are electrically small. It is not applicable for components like conductive tapes.

IV. CONCLUSIONS

This paper demonstrates a PIM simulation method, targeting solving PIM problems in complicated systems with multiple PIM sources. The nonlinear I-V and the corresponding polynomial coefficients were used to represent and adjust the nonlinearity level of the metallic contacts. By preserving the contact locations as S-parameter ports, the equivalent circuit model was extracted from a full-wave simulation. A statistical method using DoE was conducted. Following the workflow statistical results were generated and analyzed. The DoE usage in PIM study can provide strong capabilities in the engineering applications including prioritizing the locations, what-if scenario predictions, and yield analysis.

REFERENCES

- C. Hwang and J. Fan, "Modeling and Mitigation of Radio Frequency Interference for Wireless Devices," *IEEE Electromagnetic Compatibility Magazine*, vol. 12, no. 1, pp. 87-92, 1st Quarter 2023, doi: 10.1109/MEMC.2023.10136454.
- [2] Y. Sun, H. Lin, B.C. Tseng, D. Pommerenke and C. Hwang, "Mechanism and Validation of USB 3.0 Connector Caused Radio Frequency Interference," *IEEE Trans. Electromagn. Compat.*, Jul. 2019.
- [3] L. Zhang et al., "Accurate RFI Prediction of 3D Non-planar Connector with Half Magnetic Dipole Pattern," in Proc. -IEEE Asia-Pac. Symp. Electromagn. Compat., 2019.

- [4] Q. Huang et al., "Desense Prediction and Mitigation from DDR Noise Source," in Proc. of IEEE Symp. Electromagn. Compat., 2018, pp. 139-144
- [5] C. Hwang and Q. Huang, "IC placement optimization for RF interference based on dipole moment sources and reciprocity," IEEE Asia-Pacific Electromagn. Compat. Symp., 2017, pp.331-333.
- [6] Y. Sun, B.C. Tseng, H. Lin, and C. Hwang, "RFI Noise Source Quantification Based on Reciprocity," in *Proc. IEEE Int. Symp. Electromagn. Compat.*, Jul. 2018, pp. 548-553.
- [7] J. Pan, H. Wang, X. Gao, C. Hwang, E. Song, H.-B. Park, and J. Fan, "Radio-Frequency Interference Estimation Using Equivalent Dipole moment Models and Decomposition Method Based on Reciprocity," *IEEE Transactions on Electromagnetic Compatibility*, vol. 58, no. 1, pp. 75–84, 2016.
- [8] V. Golikov, S. Hienonen, and P. Vainikainen, "Passive intermodulation distortion measurements in mobile communication antennas," *IEEE 54th* Vehicular Technology Conference. VTC Fall 2001. Proceedings (Cat. No.01CH37211), Atlantic City, NJ, USA, 2001, pp. 2623-2625 vol.4, doi: 10.1109/VTC.2001.957226.
- [9] C. D. Bond, C. S. Guenzer, and C. A. Carosella, "Intermodulation generation by electron tunneling through aluminum-oxide films," *Proceedings of the IEEE*, vol. 67, no. 12, pp. 1643-1652, Dec. 1979, doi: 10.1109/PROC.1979.11544.
- [10] J. G. Simmons, "Generalized Formula for the Electric Tunnel Effect between Similar Electrodes Separated by a Thin Insulating Film," *Journal* of Applied Physics, vol. 34, no. 6, pp. 1793–1803, June 1963, doi: 10.1063/1.1702682.
- [11] J. R. Wilkerson, P. G. Lam, K. G. Gard, and M. B. Steer, "Distributed Passive Intermodulation Distortion on Transmission Lines," *IEEE Transactions on Microwave Theory and Techniques*, vol. 59, no. 5, pp. 1190-1205, May 2011, doi: 10.1109/TMTT.2011.2106138.
- [12] A. P. Shitvov, D. S. Kozlov, and A. G. Schuchinsky, "Nonlinear Characterization for Microstrip Circuits With Low Passive Intermodulation," *IEEE Transactions on Microwave Theory and Techniques*, vol. 66, no. 2, pp. 865-874, Feb. 2018, doi: 10.1109/TMTT.2017.2758726.
- [13] Q. Jin, J. Gao, L. Bi and Y. Zhou, "The Impact of Contact Pressure on Passive Intermodulation in Coaxial Connectors," *IEEE Microwave and Wireless Components Letters*, vol. 30, no. 2, pp. 177-180, Feb. 2020, doi: 10.1109/LMWC.2019.2957983.

- [14] H. Yang, H. Wen, Y. Qi and J. Fan, "An Equivalent Circuit Model to Analyze Passive Intermodulation of Loose Contact Coaxial Connectors," *IEEE Transactions on Electromagnetic Compatibility*, vol. 60, no. 5, pp. 1180-1189, Oct. 2018, doi: 10.1109/TEMC.2018.2794992.
- [15] S. Xia et al., "Practical Fixture Design for Passive Intermodulation Tests for Flexible Metallic Contacts," 2022 IEEE International Symposium on Electromagnetic Compatibility & Signal/Power Integrity (EMCSI), Spokane, WA, USA, 2022, pp. 17-22, doi: 10.1109/EMCSI39492.2022.9889578.
- [16] S. Xia et al., "Passive Intermodulation Under Different Spring Contact Conditions," 2022 IEEE International Symposium on Electromagnetic Compatibility & Signal/Power Integrity (EMCSI), Spokane, WA, USA, 2022, pp. 12-16, doi: 10.1109/EMCSI39492.2022.9889661.
- [17] Q. Jin, J. Gao, G. T. Flowers, Y. Wu, G. Xie, and L. Bi, "Modeling of Passive Intermodulation in Connectors With Coating Material and Iron Content in Base Brass," *IEEE Transactions on Microwave Theory and Techniques*, vol. 67, no. 4, pp. 1346-1356, April 2019, doi: 10.1109/TMTT.2019.2893193.
- [18] J. Li et al., "Self-contact Introduced Passive Intermodulation Characterizations for Captured Springs," 2021 IEEE International Joint EMC/SI/PI and EMC Europe Symposium, Raleigh, NC, USA, 2021, pp. 929-934, doi: 10.1109/EMC/SI/PI/EMCEurope52599.2021.9559265.
- [19] Lawson, J. (2015). Design and analysis of experiments with R. Chapman & Hall/CRC.
- [20] K. W. Anjajo et al., "Static I-V based PIM Evaluation for Spring and Fabric-over-Foam Contacts," 2023 IEEE Symposium on Electromagnetic Compatibility & Signal/Power Integrity (EMC+SIPI), Grand Rapids, MI, USA, 2023, pp. 83-87, doi: 10.1109/EMCSIPI50001.2023.10241745.
- [21] S. Xia et al., "RFI Estimation for Multiple Noise Sources Due to Modulation at a Digital Mic Using Diople Moment Based Reciprocity," 2020 IEEE International Symposium on Electromagnetic Compatibility & Signal/Power Integrity (EMCSI), Reno, NV, USA, 2020, pp. 1-5, doi: 10.1109/EMCSI38923.2020.9743517.
- [22] S. Xia et al., "Gassian Process Regression Analysis of Passive Intermodulation Level and DCR for Spring Contacts," 2021 IEEE International Joint EMC/SI/PI and EMC Europe Symposium, Raleigh, NC, USA, 2021, pp. 935-939, doi: 10.1109/EMC/SI/PI/EMCEurope52599.2021.9559359.